An Accurate Power Control Strategy for Power-Electronics-Interfaced Distributed Generation Units Operating in a Low-Voltage Multibus Microgrid

Yun Wei Li, *Member, IEEE*, and Ching-Nan Kao

***Abstract*—In this paper, a power control strategy is proposed for a low-voltage microgrid, where the mainly resistive line impedance, the unequal impedance among distributed generation (DG) units, and the microgrid load locations make the conventional frequency and voltage droop method unpractical. The proposed power control strategy contains a virtual inductor at the interfacing inverter output and an accurate power control and sharing algorithm with consideration of both impedance voltage drop effect and DG local load effect. Specifically, the virtual inductance can effectively prevent the coupling between the real and reactive powers by introducing a predominantly inductive impedance even in a low-voltage network with resistive line impedances. On the other hand, based on the predominantly inductive impedance, the proposed accurate reactive power sharing algorithm functions by estimating the impedance voltage drops and significantly improves the reactive power control and sharing accuracy. Finally, considering the different locations of loads in a multibus microgrid, the reactive power control accuracy is further improved by employing an online estimated reactive power offset to compensate the effects of DG local load power demands. The proposed power control strategy has been tested in simulation and experimentally on a low-voltage microgrid prototype.**

***Index Terms*—Distributed generation (DG), droop control method, microgrid, parallel inverter, power control, power sharing, renewable energy resource (RES).**

I. Introduction

With the increased concerns on environment and cost of energy, the power industry is experiencing fundamental changes with more renewable energy sources (RESs) or microsources such as photovoltaic cells, small wind turbines, and microturbines being integrated into the power grid in the form of distributed generation (DG). These RES-based DG systems are normally interfaced to the grid through power electronics and energy storage systems [1].

A systematic organization of these DG systems forms a microgrid [2]–[7]. Compared to a single DG, the microgrid has more capacity and control flexibilities to fulfill system reliability and power quality requirements. The microgrid also offers opportunities for optimizing DG through the combined heat and power (CHP) generation, which is currently the most important means of improving energy efficiency. By presenting itself to the utility as a dispatchable load, the microgrid could "behave" well and avoid problems caused by single DG units [2]. Furthermore, the microgrid can operate in grid-connected mode or autonomous islanding mode and benefits both the utility and customers. Depending on the locations and capacities of DG units, a microgrid could operate at a medium-voltage or low-voltage distribution level. Since most microsources are of relatively low-power capacities at around several hundred kilowatts, a low-voltage microgrid is considered in this paper.

With a nonradial system configuration due to the presence of DG units, the power control complexity for a microgrid is substantially increased, and the "plug and play" feature is the key to ensure that the installation of additional DG units will not change the control strategies of DG units already in the microgrid. A popular approach to realize this "plug and play" characteristic is to employ the frequency and voltage droop control for real and reactive power regulation by mimicking the parallel operation characteristics of synchronous generators, which is initially proposed in [8] for parallel uninterruptible power supply (UPS) operations. While the stability analysis of this droop control is an important aspect as discussed recently in [9], [10], when implemented in a low-voltage microgrid system, this method is subject to a few particular problems, which are as follows.

1) The method is developed based on the predominantly inductive line impedance. In a low-voltage microgrid, as the distribution feeder is mainly resistive, this droop method is subject to poor transient (or even poor stability) due to the real and reactive power coupling among DG units when no additional inductance is present.
2) The unequal line impedances and DG output impedances significantly affect the accuracy of reactive power control during grid-connected operation mode and the reactive power sharing during islanding mode due to the unequal voltage drops.
3) The reactive power sharing accuracy is further deteriorated if there are local loads at DG output.

To avoid the power control coupling, the virtual real and reactive power frame transformation was recently proposed [11]. However, this method cannot directly share the actual real and reactive powers. Another way to avoid the power coupling is to properly control the interfacing inverter with virtual output impedance [12]–[14]. While effective in preventing the power coupling, this approach may increase the reactive power control

Manuscript received February 25, 2009; revised April 1, 2009. Current version published December 28, 2009. This paper will be presented in part at the 1st IEEE Energy Conversion Congress and Exposition (ECCE), San Jose, CA, September 20–24, 2009. Recommended for publication by Associate Editor R. Teodorescu.

The authors are with the Department of Electrical and Computer Engineering, University of Alberta, Edmonton, AB T6G 2V4, Canada (e-mail: yunwei.li@ece.ualberta.ca).

Color versions of one or more of the figures in this paper are available online at http://ieeexplore.ieee.org.

Digital Object Identifier 10.1109/TPEL.2009.2022828

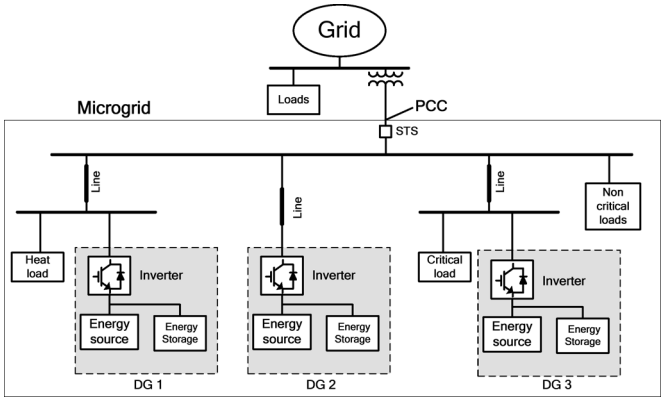

Fig. 1. Example microgrid with power electronics interfaced DG systems.

and sharing error due to the increased impedance voltage drops. To improve the reactive power sharing accuracy, a method has been proposed based on additional control signal injection [15]. However, this method has a few disadvantages such as increased control complexity and possible line current distortions.

In this paper, a power control strategy is developed for the low-voltage microgrid. The strategy comprises a virtual inductor at the interfacing inverter output and an accurate reactive power control and sharing algorithm with consideration of impedance voltage drop and DG local load effects. Specifically, the virtual inductance can effectively prevent the coupling between real and reactive powers by presenting a mainly inductive impedance even in a low-voltage network with resistive line impedances. This is done without physically connecting any passive components at the DG output. On the other hand, based on the predominantly inductive impedance, the proposed accurate reactive power sharing algorithm functions by estimating the impedance voltage drop to reactive power ratio and significantly improves the reactive power control and sharing accuracy. Finally, considering the complex locations of loads in a multibus microgrid, the reactive power control accuracy is further improved by employing an online estimated reactive power offset to compensate the effects of DG local load power demands. The proposed power control strategy has been tested in MATLAB/Simulink simulation and experimentally on a low-voltage experimental microgrid system.

II. Microgrid Structure

An example structure of a microgrid is shown in Fig. 1. The microgrid is connected to the utility system through a static transfer switch (STS) at the point of common coupling (PCC). The STS ensures that the microgrid can be disconnected from the main grid promptly (typically half a line frequency cycle) in the event of a utility interruption. As shown in Fig. 1, three DG systems are employed in the microgrid. Each DG system comprises an energy source, an energy storage system, and a grid-interfacing inverter. In Fig. 1, DG1 is connected near a heat load for CHP application, DG3 is connected with a local critical load, and DG2 is connected to the feeder directly for voltage and power support. This microgrid structure allows the line loss reduction, local voltage and power support, and waste heat usage.

The microgrid can operate in grid-connected mode or islanding mode. In grid-connected operation, the microgrid is connected to the utility, and the DG systems in the microgrid provide heat and power support for the nearby loads. When there is a fault in the utility system, the STS at PCC opens and the microgrid is disconnected from the utility as fast as possible and picks up the loads and operate in islanding mode. The STS is preferably controlled independently with a central control or power management unit, which constantly monitors the utility voltage condition and opens the switch in the case of a utility fault.

Once transferred to islanding operation, the DG systems must immediately share the changed power demand and continue supplying power to all critical loads within the microgrid. Also, the least important loads can be shed if the power capacity of the microgrid is insufficient to support all the loads in it. Note that if a single-direction communication from the STS (or central control unit) to a DG unit is not available, an islanding detection algorithm has to be implemented in this DG unit to ensure a successful transition of microgrid operation from grid-connected mode to islanding mode [7], [16]. When the utility voltage is back to normal condition, for smooth connection of the microgrid and utility, synchronization of the two systems can be done by monitoring the voltages at both ends of the STS and closing the switch when the two voltages are in phase. More advanced "seamless" synchronization that guarantees a perfect match of both voltage magnitude and phase angle could also be realized if the single-direction communication from the central control unit to the DG units is available, where the synchronization reference signal can be sent from the central control to the DG units [4] (note that communication among the DG units is unnecessary).

This multibus microgrid structure increases the complexity of power and voltage control along the feeder. Therefore, the "plug and play" concept or "wireless communication" is the key to this arrangement. To realize this "plug and play" characteristic, conventional power and frequency droop power control methods have been implemented in [4]. However, as mentioned previously, the conventional droop method is subject to a number of issues such as a coupling between real and reactive powers at a low-voltage microgrid with resistive line impedances and degradation of reactive power control accuracy in both grid-connected and islanding operations.

III. Traditional Frequency and Voltage Droop Method

A. Frequency and Voltage Droop Control

A well-known method to realize the "plug and play" feature for each DG unit is to control the DG terminal voltage by employing the "real power versus frequency (P–ω)" and "reactive power versus voltage (Q–E)" droop control [8]. Put simply, this method is based on the flow of real power and reactive power (per phase) between two nodes separated by a line impedance

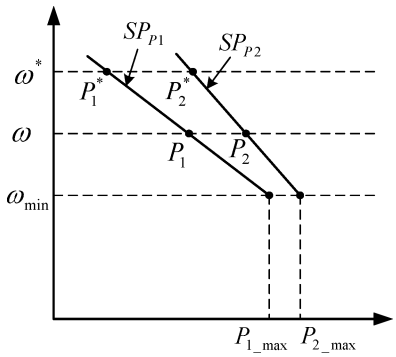

Fig. 2. Real power sharing through frequency droop control.

$(Z = R + jX)$ as

$$P = \frac{E_1}{R^2 + X^2}[(R(E_1 - E_2\cos\delta) + XE_2\sin\delta] \quad (1)$$

$$Q = \frac{E_1}{R^2 + X^2}[-RE_2\sin\delta + X(E_1 - E_2\cos\delta)] \quad (2)$$

where E_1 and E_2 are the magnitudes of the two voltages, and δ is the phase angle difference between the two voltages. For a mainly inductive line impedance, the line resistance (*R*) may be neglected. Further, considering that the phase angle difference δ is typically small, it is reasonable to assume $\sin(\delta) = \delta$ and $\cos(\delta) = 1$. Therefore, the flow of real power is proportional to the phase angle difference (δ) and the flow of reactive power is proportional to the voltage magnitude difference ($E_1 - E_2$). For this reason, the real power from each DG unit can be controlled by varying the DG output frequency, and hence, the phase angle and the DG reactive power can be regulated by changing the DG output voltage magnitude. This control concept could be used in both the grid-connected and islanding operation modes.

Fig. 2 shows the *P–ω* droop characteristics for two DG systems (note that the control strategy is equally applicable to a microgrid with more DG units). Preferably, these droop characteristics should be coordinated to make each DG system supplying real power in proportion to its power capacity, and can mathematically be expressed as

$$\omega_i = \omega^* - SP_{P_i}(P_i^* - P_i) \quad (3)$$

$$SP_{P_i} = \frac{\omega^* - \omega_{\min}}{P_i^* - P_{i\_\max}} \quad (4)$$

where P_i is the actual real power output of DG system *i* ($i = 1$, 2,. . ., *n*), $\{P_{i\_\max}, \omega_{\min}\}$ are the maximum real power output of DG system *i* and the minimum allowable operating frequency, $\{P_i^*, \omega^*\}$ are the dispatched real power and operating frequency of DG system *i* in grid-connected mode, and SP_{P_i} (<0) is the slope of the droop characteristics.

As shown in Fig. 2, each DG system is initially designed to generate the dispatched real power output of P_i^* at the common base frequency of ω^* when operating in the grid-connected mode (ω^* is fixed solely by the stiff utility grid). Once islanded, the power outputs of both DG systems must immediately be changed in accordance with their droop characteristics to supply power to all critical loads in the microgrid at a new steady-state frequency of ω. This arrangement obviously allows both DG systems to share the total load demand in a predetermined manner according to their respective power ratings.

In a similar manner, the magnitude set point of each DG output voltage can be tuned according to a specified *Q–E* droop scheme to control the flow of reactive power within the microgrid. Mathematically, the *Q–E* characteristics can be expressed as

$$E_i = E^* - SP_{Q_i}(Q_i^* - Q_i) \quad (5)$$

$$SP_{Q_i} = \frac{E^* - E_{\min}}{Q_i^* - Q_{i\_\max}} \quad (6)$$

where Q_i is the actual reactive power output of DG system *i*, $\{Q_{i\_\max}, E_{\min}\}$ are the maximum reactive power output and minimum allowable voltage magnitude of the microgrid, $\{Q_i^*, E^*\}$ are the dispatched reactive power of DG system *i* and PCC voltage magnitude when in grid-connected mode, and SP_{Q_i} is the slope of the droop characteristics. Conceptually similar to the *P–ω* operation, the accuracy of reactive power control and sharing is, however, subject to the voltage drop on line impedances, as discussed later.

B. Power Coupling at Low-Voltage Microgrid

While working well in a power grid with mainly inductive line impedances, the traditional real and reactive power control (where the line resistance is neglected) leads to a concern when implemented on a low-voltage microgrid, where the feeder impedance is not inductive and the line resistance (*R*) should never be neglected. This is especially true for DG units without a grid-side inductor or transformer, where the output inductance is very small. In this case, the change of phase angle or voltage magnitude will influence both the real power and reactive power flows, as can be noticed from (1) and (2). As a result, controlling the power flow using conventional *P–ω* and *Q–E* droop methods will introduce a significant coupling between the real and reactive power flows especially during transients.

To avoid this *P–Q* coupling, virtual real and reactive powers can be used, which are decoupled through frame transformations with the line impedance angle information [11]. While effective for power control in grid-connected mode, this method cannot directly share the actual real and reactive powers between the DG units in microgrid islanding operation mode. Another way to decouple the powers with direct power control is to employ the virtual voltage and frequency control frame [17]. Unfortunately, these frame transformation methods are still subject to the accuracy of the power control due to unequal impedance voltage drops. In order to control the decoupled real and reactive power flows in a similar manner as the conventional power system with a high *X/R* ratio, a method employed in this paper is to control the DG interfacing inverter with a virtual output inductor that introduces a predominantly inductive impedance without the need of line impedance information. The virtual inductance can effectively decouple the real and reactive power flows and requires no physical connection of any passive components at the DG output. With a virtual inductor at each DG's output, the conventional *P–ω* and *Q–E* methods can be used,

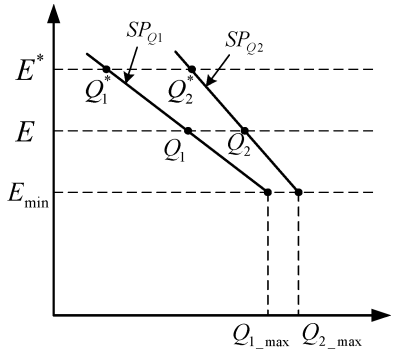

Fig. 3. Reactive power sharing with traditional voltage droop control.

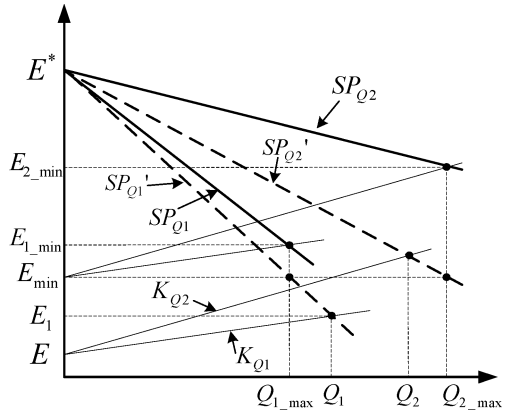

Fig. 4. Reactive power sharing diagram with line impedance (inductive) effects.

which makes the power sharing algorithm equally applicable even when the rotational machine based DG units (where the *P–ω* and *Q–E* characteristics are determined by the mechanical governor and excitation system, respectively) are present in a microgrid. Note that although the impedance voltage drop effect is more severe with the virtual inductance control, this effect can be estimated and properly compensated.

C. Inaccuracy of Reactive Power Control Due to Line Impedance

Unlike the *P–ω* control where the DG systems and utility grid have the same steady-state frequency in the grid-connected mode, allowing the same *P–ω* control algorithm to be used for both the grid-connected and islanding modes, a complication with the *Q–E* droop control is that the DG output voltage has to be different from that of the utility grid to introduce a voltage magnitude difference, and therefore, allows proper reactive power flow in grid-connected operation. As a result, the *Q–E* droop scheme specified in (5) and (6) will lead to reactive power control error. One way to solve this complication is to add an additional integral or PI reactive power compensator for use in grid-connected mode [4], [18], [19] (see Fig. 8). When connected to the utility grid, only the PI compensator is selected for reactive power control, forcing the DG reactive power output to track its dispatched value with zero steady-state error. When the microgrid transfers to islanding operation, the reactive power control scheme can be switched to the *Q–E* droop control for proper reactive power sharing among the DG units (see Fig. 3).

For a similar reason, a second complication with the *Q–E* droop control is that the reactive power sharing accuracy is affected by the line impedance voltage drop. This phenomenon is illustrated in Fig. 4, where the predominantly inductive line impedance is assumed that leads to an approximately linear relationship between the DG output reactive power and the voltage magnitude difference (between DG output voltage and PCC voltage) ΔE, as can be noticed from (2). This linear relationship for DG system *i* can be expressed as

$$K_{Q_i} = \frac{\Delta E}{Q_i} = \frac{X_i}{E_i} \tag{7}$$

where K_{Q_i} is the slope of DG output voltage magnitude difference ΔE versus reactive power (note that K_{Q_i} should be scaled down by a factor of 3 for a three-phase system). As the DG output voltage is limited to vary only in a small range (e.g., $\pm 10\%$) and the inductance between two voltages is normally a constant, it is reasonable to assume K_{Q_i} as a constant slope.

To simplify the illustration, it is first assumed that the power factor of the two DGs is unity with zero reactive power output in grid-connected mode, and the two DGs share the load reactive power demand only in islanding mode. Without considering the line voltage drop, the voltage droop slopes of the two DG systems defined by (5) and (6) are shown by the dashed lines (SP'_{Q_1} and SP'_{Q_2}) in Fig. 4. It can be seen that if the dashed lines are used for reactive power sharing, when the two DG units supply the maximum total reactive power to the loads, DG2 output reactive power (Q_2) will be smaller than its maximum value ($Q_{2\_\max}$), and the DG1 output reactive power (Q_1) will be larger than its maximum value ($Q_{1\_\max}$). This reactive power sharing inaccuracy leads to a risk of exceeding the DG system current ratings. Furthermore, it can be seen in Fig. 4 that with the slopes determined in (5) and (6), the final minimum system voltage (PCC voltage) will be smaller than the minimum allowable voltage ($E_{\min}$), which is unacceptable to the sensitive loads.

With the consideration of the line impedance effects and the $\Delta E/Q$ slopes defined in (7), the voltage droop slopes can be redefined to be SP_{Q_1} and SP_{Q2}, as shown by the solid lines in Fig. 4, where the minimum allowable DG output voltage and the *Q–E* droop slope of each DG system can be obtained as

$$E_{i\_\min} = E_{\min} + K_{Q_i} Q_{i\_\max} \tag{8}$$

$$SP_{Q_i} = \frac{E^* - E_{i\_\min}}{-Q_{i\_\max}}. \tag{9}$$

With (8) and (9), both DG units will provide the maximum reactive power at the minimum allowable system voltage. More details on the accurate reactive power sharing are discussed in Section V.

IV. Virtual Inductance for *P–Q* Decoupling

This section presents the interfacing inverter control scheme with virtual output inductance, which provides a mainly

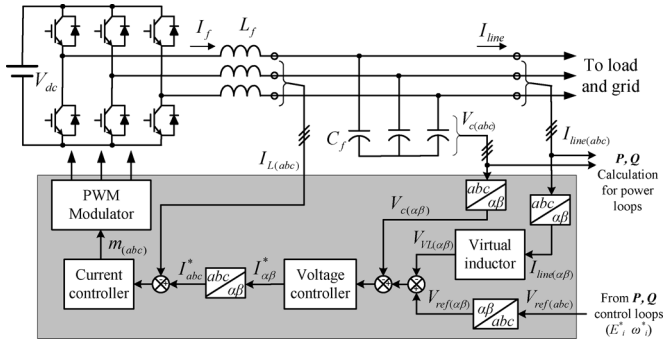

Fig. 5. Voltage control scheme for the DG interfacing inverter.

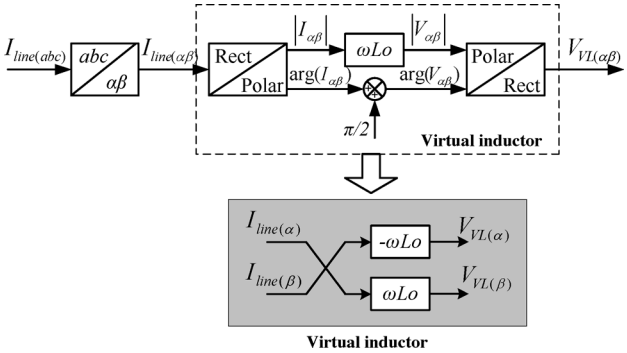

Fig. 6. Virtual inductor realization scheme.

inductive impedance between the DG and the utility even in a low-voltage network with resistive line impedances.

Fig. 5 shows the interfacing inverter voltage control scheme. As shown, the reference voltage for the inverter comes from the real and reactive power control loops, which determine the DG output voltage magnitude and frequency. For the inverter voltage control, a multiloop control scheme is implemented, where an inner filter inductor current (I_L) feedback loop is embedded in an outer filter capacitor voltage (V_c) feedback loop. Both the voltage and current controllers are implemented on the stationary frame to avoid the complex frame transformations. For the voltage loop, the $P+$ resonant controllers in the form of (10) are employed in the α–β frame [20]–[22]

$$G(s) = k_P + \frac{2k_I\omega_C s}{s^2 + 2\omega_C s + \omega_0^2} \tag{10}$$

where k_P is the proportional gain, k_I is the resonant gain for the resonant peak adjustment, and ω_C is the cutoff frequency for resonant bandwidth control. The controller in (10) is actually a practical form of the ideal $P+$ resonant controller that can be mathematically derived by transforming a synchronous frame PI controller to the stationary frame. It is worth noting that (10) ensures almost zero steady-state error regulation by having significant gains in the vicinity of the controller's resonant frequency $\pm\omega_0$, which, in this case, is chosen to be the line fundamental frequency. Output of the voltage controller is then transformed to the *a–b–c* frame to generate the reference current I_L^* for the inner filter inductor current loop. The current error is fed to a proportional controller whose output gives the desired modulation signal and is fed to the pulsewidth-modulated (PWM) generator.

To emulate the effect of an inductor, the line current is fed back to calculate the virtual inductor voltage drop (V_{VL}), which is then subtracted from the reference voltage (generated from the power loops) to produce the final inverter voltage reference. A concern for the virtual inductor control scheme is the inductor voltage drop calculation, which involves the differentiation of line current ($V_{VL} = L_0(di_{\text{line}}/dt) = sL_0 i_{\text{line}}$, where L_0 is the virtual inductance value). Differentiation can cause high-frequency noise amplification, which in turn may destabilize the DG voltage control scheme especially during a transient. A common approach to avoid noise amplification is to add a high-pass filter to flatten the high-frequency gain of the resulting transfer function [13], [14]. However, this approach is subject to the tradeoff between the high-frequency noise attenuation and the fundamental component phase and gain errors (or the tradeoff between overall control scheme stability and the virtual inductor control accuracy).

As the power control in this paper is based on the fundamental component, a more robust approach to determine the virtual inductor voltage drop is, therefore, proposed to avoid the differentiation by approximating sL_0 as $j\omega L_0$, where ω is the system angular frequency. This $j\omega L_0$ representation can be realized in polar form with polar–rectangular transformations or through direct complex number manipulations in the α–β frame. Both methods are illustrated in Fig. 6. For the polar–rectangular form transformations, the measured three-phase currents are first transformed to the α–β frame and converted to the polar form of $|I_{\alpha\beta}|\angle\arg(I_{\alpha\beta})$, where $|I_{\alpha\beta}| = \sqrt{I_\alpha^2 + I_\beta^2}$ and $\arg(I_{\alpha\beta}) = \tan^{-1}(I_\beta/I_\alpha)$. Multiplying $I_{\alpha\beta}$ by the desired virtual inductance $j\omega L_0$ gives the desired inductor voltage drop (in polar form) of $|V_{\alpha\beta}| = |I_{\alpha\beta}|\omega L_0$, and $\arg(V_{\alpha\beta}) = \arg(I_{\alpha\beta}) + (\pi/2)$, which is subsequently transformed back to rectangular form of $V_{VL(\alpha\beta)}$. On the other hand, for the complex number manipulations in the α–β frame, as shown in the shaded part of Fig. 6, the α–β frame voltage drop can be directly found from the line current with $(V_\alpha + jV_\beta) = j\omega L_0(I_\alpha + jI_\beta) = \omega L_0(-I_\beta + jI_\alpha)$, where the magnitude and angle calculations required in the polar–rectangular form transformations can be avoided.

V. Reactive Power Control Algorithm With Improved Accuracy

As mentioned in Section III, the reactive power control and sharing based on the traditional voltage droop method are inaccurate due to the voltage drop in the line impedances. One method to improve the accuracy is to exaggerate the *Q–E* droop effect and make the line voltage drop negligible [23]. However, with a given minimum allowable system voltage, the voltage droop slope cannot be made arbitrarily large. As mentioned previously, a better way to improve the reactive power control and sharing accuracy is to incorporate the line voltage drop effect into the power control scheme. This can be realized by adding the $\Delta E/Q$ slopes into the voltage droop control. It is

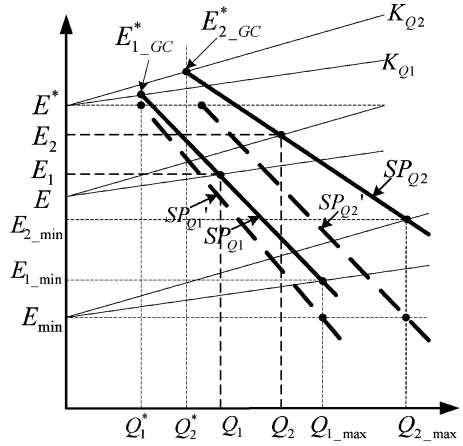

Fig. 7. Reactive power flows of two DGs with consideration of their $\Delta E/Q$ (K_{Q_i}) slopes.

worth mentioning that with the controlled virtual inductor at each DG's output, the $\Delta E/Q$ slope in (7) can be effectively employed for reactive power control accuracy improvement. In other words, the virtual inductor control not only decouples the real and reactive power flows, but it also enables the reactive power control accuracy improvement by properly defining the $\Delta E/Q$ slope at each DG's output. Note that with the output virtual inductor, the DG output voltage refers to the voltage before the virtual inductor, which is related to the voltage reference generated from the real and reactive power control loops ($V_{\rm ref}$, see Fig. 5).

A. Proposed Accurate Reactive Power Control Method

Fig. 7 shows the reactive power control and sharing diagram of a microgrid with two DG systems. Compared to Fig. 4, Fig. 7 shows a more general case where the DG systems might not necessarily operate with unity power factor (when reactive power compensation is needed) and the DG output reactive power in grid-connected mode is nonzero. As mentioned in Section III, for reactive power flow control in grid-connected operation, a PI controller can be used that compensates the impedance voltage drop and ensures zero steady-state reactive power regulation. As illustrated in Fig. 7, during grid-connected operation, the PCC voltage is E^*, and the two DGs output voltages are $E^*_{1\_\rm GC}$ and $E^*_{2\_\rm GC}$, respectively.

On the other hand, the accuracy of reactive power sharing in islanding microgrid operation can be improved by incorporating the $\Delta E/Q$ slope K_{Q_i} and modifying the voltage droop slope. As shown in Fig. 7, if the $\Delta E/Q$ slope is not considered, the voltage droop slopes are the dashed lines (SP'_{Q_i}), which may lead to one or more DG units generating reactive power beyond the maximum limit, as explained earlier. While if K_{Q_i} is considered when determining the desired *Q–E* droop slope (SP_{Q_i}) for each DG unit, the two DGs simultaneously generate their respective maximum reactive power under the maximum load reactive power demand, and at the same time, the minimum system voltage (PCC voltage) is $E_{\rm min}$. As a result, the risks of operating DG systems beyond the maximum rating and the microgrid voltage dropping below the minimum allowable value can be minimized. To realize this accurate power sharing, the DG output voltage magnitude reference E^*_i and the voltage droop slope SP_{Q_i} can be calculated as in (11) and (12), respectively, where $E_{i\_\rm min}$ in (12) is determined in a similar manner as in (8)

$$E^*_i = E^*_{i\_\rm GC} - SP_{Q_i}\,(Q^*_i - Q_i) \tag{11}$$

$$SP_{Q_i} = \frac{E^*_{i\_\rm GC} - E_{i\_\rm min}}{Q^*_i - Q_{i\_\rm max}}. \tag{12}$$

B. Power Controller Realization

The performance of the accurate reactive power control and sharing algorithm highly depends on the obtained $\Delta E/Q$ slope K_{Q_i} at each DG output. As illustrated in (7), the slope K_{Q_i} is related to the system voltage, and the impedance between the DG and the PCC. As the microgrid voltage is not allowed to vary in a wide range, it can be concluded that the accuracy of K_{Q_i} and therefore the reactive power sharing accuracy, mainly depend on the estimation of reactance at each DG's output. For a low-voltage microgrid, where the line inductance is very small, the virtual inductance implemented on each DG's interfacing inverter is the predominant inductance between the DG and PCC. As a result, K_{Q_i} can be accurately obtained as the virtual inductance is a known parameter in the inverter voltage control scheme. To further improve the accuracy of obtained K_{Q_i}, an online slope estimation scheme is proposed, which makes the accurate reactive power sharing algorithm even suitable for DG units with a grid-side inductor or transformer, or a medium-voltage microgrid with mainly inductive line impedances (without virtual inductor control).

Fig. 8 shows the proposed reactive power control scheme for each DG system. It contains a PI control loop for use with grid-connected mode of operation, a voltage droop control loop for use in islanding operation, and an online K_{Q_i} slope estimation algorithm. Specifically, the PI controller in the grid-connected mode ensures reactive power regulation with zero steady-state error. The voltage droop control [as described in (11)] in islanding mode enables accurate reactive power sharing among the DG units in a microgrid according to their respective ratings and the minimum allowable system voltage. The online slope estimation algorithm estimates the $\Delta E/Q$ slope (K_{Q_i}) of each DG, with which the accurate *Q–E* droop slope (SP_{Q_i}) can be determined, as in (12) and Fig. 7.

As shown in Fig. 8, the $\Delta E/Q$ slope (K_{Q_i}) of each DG is estimated during the DG's grid-connected operation. At steady-state grid-connected operation, the DG output reactive power is equal to the dispatched reactive power Q^*_i, and the difference between the DG output voltage and the grid voltage (PCC voltage) is actually the PI controller's output ($\Delta E = E^*_i - E^*$). The $\Delta E/Q$ slope can therefore be obtained as ($K_{Q_i} = (E^*_i - E^*)/Q^*_i$). A low-pass filter (LPF) is applied to smoothen the obtained slope (K_{Q_i}), which is subsequently used to calculate the DG's *Q–E* droop slope. During steady-state operation, when the obtained slopes K_{Q_i} and SP_{Q_i} are stabilized, the value can be stored for used in islanding mode. Once a fault occurs in the utility and

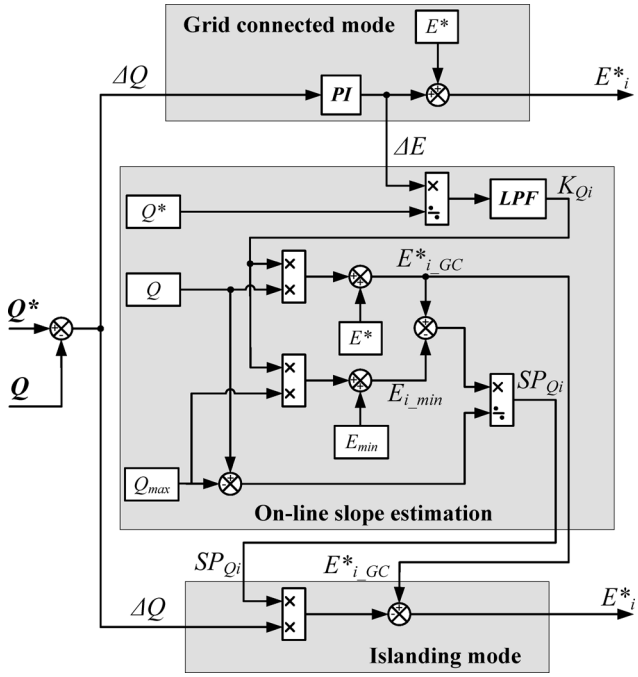

Fig. 8. Proposed reactive power control and sharing scheme.

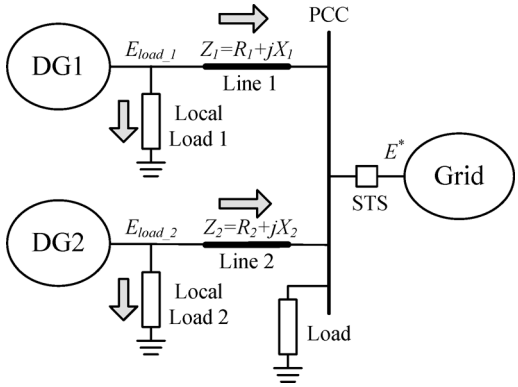

Fig. 9. Two parallel DGs connected to the grid with local loads.

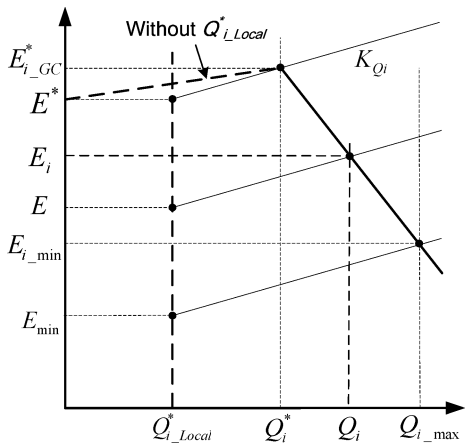

Fig. 10. *Q–E* relationship with DG local loads.

the microgrid is transferred to islanding operation mode, the obtained *Q–E* droop slope (SP_{Q_i}) can then be used for accurate reactive power sharing control.

A complication anticipated with the slope estimation scheme is the unity power factor DG operation ($Q_i^* = 0$) in grid-connected mode. In this case, both the dispatched DG reactive power output and the PI controller output are zero. One option under this situation is to use the value of virtual inductor at each DG's output to estimate the slope K_{Q_i} as discussed before. In order to accurately estimate the slope (K_{Q_i}) online, the DG can be controlled with a small reactive power output for a very short period (as long as the power reaches steady state). After the slopes K_{Q_i} and SP_{Q_i} are obtained, the DG reactive power output in grid-connected mode can be reset to zero for unity power factor operation.

VI. Compensation of DG Local Load Effects

The reactive power sharing discussed so far is based on the reactive power flow between two voltages separated by an impedance. However, in a multibus microgrid, the location of microgrid loads will also affect the power flows.

Fig. 9 shows a microgrid with two DG systems where each DG system has a local load connected directly at the DG output. The exact same control scheme for grid-connected operation (with integral control of reactive power to compensate impedance voltage drops) can be used for DG systems with local loads. Similarly, in islanding operation, since the DG systems will operate at the same frequency, the real power sharing based on P–ω droop is not affected by the DG local loads. However, the local loads will affect the reactive power sharing performance during islanding operation. An obvious phenomenon is that when the DG local load voltage (E_{load_i}, which is corresponding to V_c in Fig. 5) is equal to the PCC voltage (E^*), the DG output reactive power is not zero, and it is the local load reactive power demand instead. Therefore, the DG local load introduces an offset in the DG output voltage and reactive power relationship. This offset, if not properly considered, will significantly affect the accuracy of estimated slopes of K_{Q_i} and SP_{Q_i} and, therefore, affect the accuracy of reactive power sharing in islanding operation.

To compensate the effects of DG local loads, an offset has to be added to each DG's output reactive power and voltage relationship, as shown in Fig. 10, where the reactive power offset caused by the DG local load is shown as $Q^*_{i\_\text{Local}}$. It can be seen that if the local load effects are not considered, the estimated $\Delta E/Q$ slope will deviate from the actual slope K_{Q_i} and, therefore, affect the accuracy of reactive power sharing. When the reactive power offset is larger than the dispatched reactive power ($Q^*_{i\_\text{Local}} > Q^*_i$), the estimated slope will even be a negative value if the offset is not considered. With proper consideration of the reactive power offset effects, the $\Delta E/Q$ slope of a DG unit can be determined by

$$K_{Q_i} = \frac{E^*_{i\_\text{GC}} - E^*}{Q^*_i - Q^*_{i\_\text{Local}}}. \tag{13}$$

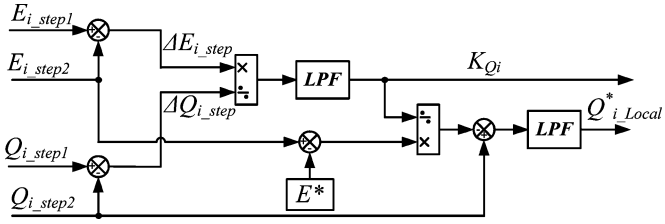

Fig. 11. K_{Q_i} and reactive power offset ($Q^*_{i\_\mathrm{Local}}$) estimation diagram.

With the correct $\Delta E/Q$ slope, the voltage droop slope and DG output voltage can be controlled as in (11) and (12), with the only difference being that the minimum DG output voltage in (12) should be determined as in (14) [instead of (8)], considering the DG local load effects

$$E_{i\_\min} = E_{\min} + K_{Q_i}(Q_{i\_\max} - Q^*_{i\_\mathrm{Local}}). \tag{14}$$

It should be noted that the reactive power offset $Q^*_{i\_\mathrm{Local}}$ is not necessarily the local load reactive power demand, especially when the DG interfacing inverter is controlled with an output virtual inductor (note the difference between the reference voltage from power loops and the inverter reference voltage after the virtual resistor in Fig. 5). In this case, the reactive power offset is related to the line impedance parameters, the virtual inductance, and finally, the local load power demand. As the information of the line impedances and local load demands might not be accurately obtained, an alternative way to estimate the reactive power offset for each DG system is proposed here, which is incorporated into a modified slope K_{Q_i} estimation algorithm, as shown in Fig. 11.

Unlike the slope estimation in Fig. 8, the one-step estimation at steady-state grid-connected operation cannot accurately estimate the value of K_{Q_i} if the reactive power offset effects are considered (it will only generate the dashed slope as illustrated in Fig. 10). To accurately estimate both the slope K_{Q_i} and the reactive power offset $Q^*_{i\_\mathrm{Local}}$, two-step estimation method, as illustrated in Fig. 11, can be conducted, where the information of DG reactive power output at two steady-state operation steps (Q_{i_step1} and Q_{i_step2}) and the respective DG output voltages (E_{i_step1} and E_{i_step2}) are obtained. Once again, the LPFs in Fig. 11 are used to smoothen the obtained variables. The slope and the reactive power offset estimation in Fig. 11 can be expressed in (15) and (16), respectively. Note that the reactive power offset in (16) can also be obtained with the voltage and reactive power for the first-step operation (E_{i_step1} and Q_{i_step1})

$$K_{Q_i} = \frac{\Delta E}{\Delta Q} = \frac{E_{i\_\mathrm{step2}} - E_{i\_\mathrm{step1}}}{Q_{i\_\mathrm{step2}} - Q_{i\_\mathrm{step1}}} \tag{15}$$

$$Q^*_{i\_\mathrm{Local}} = Q_{i\_\mathrm{step2}} - \frac{E_{i\_\mathrm{step2}} - E^*}{K_{Q_i}}. \tag{16}$$

The two-step estimation can be simply performed during the starting of the DG in grid-connected mode by increasing the DG output reactive power to its dispatched value in two steps such as 0 and Q^*_i (or $Q^*_i/2$ to Q^*_i), which results in $E_{i\_\mathrm{step2}} = E_{i\_\mathrm{GC}}$ and $Q_{i\_\mathrm{step2}} = Q^*_i$. As long as the DG reaches the steady-state operation in the first step (which is very fast and is about 0.5 s in this paper), the voltage and reactive power information can be stored and the DG can move on to the second step (the final dispatched reactive power in grid-connected mode). Note that this DG starting practice by increasing the DG reactive power output in two separate steps could also give the advantage of smoother DG starting transients.

Finally, with the slope K_{Q_i}, the reactive power offset $Q^*_{i\_\mathrm{Local}}$, and the minimum DG output voltage $E_{i\_\min}$, the accurate voltage droop slope SP_{Q_i} can be calculated using (12). The online slope estimation diagram in Fig. 8 can then be replaced by the algorithms discussed in this section. It is worth mentioning that the reactive power offset can also compensate the possible small deviation of the stiff grid voltage from its nominal value or any slight inaccuracy in the inverter voltage control (e.g., due to voltage sensing error, voltage control error, etc.), as the voltage error will result in the reactive power flow similar to the local load effects.

VII. Further Compensation of Voltage Drop Due to Real Power Flow

The reactive power control algorithms discussed so far are based on the assumption that the real power flow only depends on the phase angle difference, which will not cause any voltage drop on the line or virtual inductance. This is untrue when considering the nontrivial line resistance in a low-voltage microgrid. Indeed, this voltage drop due to real power flow will affect the reactive power sharing performance. To compensate the effects of voltage drop due to real power flow, the following more accurate approximation of line voltage drop can be considered:

$$\Delta V = \frac{PR + QX}{E^*}. \tag{17}$$

It can be seen that the real power and together with line resistance will cause a voltage drop, which can be expressed as

$$\Delta V_{P_i} = k_{VP_i}(P_i - P_{i\_\mathrm{local}}) \tag{18}$$

where $k_{VP_i} = (R/E^*)$, and P_i and P_{i_local} are, respectively, the real power output and real power offset due to local load demand for DG unit *i*.

Note that in (18), the DG real power offset can be omitted. This is because the voltage variation due to this real power offset ($k_{VP_i}P_{i\_\mathrm{local}}$) is a constant, which has a similar effect as the reactive power offset, and therefore, can be combined into the reactive power offset estimation. As a result, only the slope k_{VP_i} should be determined to compensate the voltage variation due to real power flow. This can be done in a similar manner as discussed for the reactive power online slope and local power estimation. For example, during starting of the DG, the real power command can be increased at two steps with the second step being the final reference power. Then, by detecting the variation of DG output voltage in these two steps, the slope k_{VP_i} can be determined. During this real power to voltage drop slope estimation process, the reactive power command should be kept as constant (e.g., staying at zero). In addition, this k_{VP_i} estimation should be done before the estimation of voltage droop slope and reactive power offset in order to improve the combined real and

TABLE I
SIMULATION AND EXPERIMENT SYSTEM PARAMETERS

Parameter	Values
Nominal utility line-line voltage (rms)	104V
Minimum microgrid line-line voltage	98V
Nominal utility frequency	60Hz
Minimum microgrid frequency	59.5Hz
Maximum DG powers	500W, 225Var
Dispatched powers in grid-connected mode	175W, 75Var
DC link voltage	230V
Inverter Switching frequency	4.5kHz
Inverter output filter inductance	5mH
Inverter output filter capacitance	40μF
DC link capacitance	1900μF
DG1 virtual inductance	4mH
DG2 virtual inductance	2mH
Lines 1 and 2 (see Fig. 9)	1Ω, 0.25mH

reactive power offset accuracy. With the obtained voltage drop to real power ratio k_{VP_i}, the local DG reactive power can be modified as in (19), where $\Delta V_{P_i} = k_{VP_i} P_i$ is calculated using the DG real power output during $Q^*_{i\_\mathrm{Local}}$ estimation

$$Q^*_{i\_\mathrm{Local}} = Q_{i\_\mathrm{step2}} - \frac{E_{i\_\mathrm{step2}} - E^* - \Delta V_{P_i}}{K_{Q_i}}. \tag{19}$$

Finally, the voltage magnitude reference determined by reactive power sharing in (11) can be modified into (20) when considering the DG real power output in islanding operation

$$E^*_i = E^*_{i\_\mathrm{GC}} - SP_{Q_i}\,(Q^*_i - Q_i) + k_{VP_i} P_i. \tag{20}$$

VIII. SIMULATION RESULTS

The proposed power control strategy has been verified in MATLAB/Simulink simulations and experimentally. In the simulations and experiments, a microgrid with two DG systems, as shown in Fig. 9, is employed. The system parameters for simulation and experiment are chosen to be the same, as shown in Table I. Also in the simulations and experiments, the two DG units are designed with identical parameters to facilitate the observation of the power sharing accuracy. However, the virtual inductance values are intentionally selected to be different (DG1: 4mH and DG2: 2mH; see Table I) to introduce the effects of unequal impedance voltage drops.

Fig. 12 shows the real and reactive power flows (note that the powers are calculated from the DG output voltages and line currents; see Fig. 5) of the two DG systems in the scenario of no DG local loads (Load 1 and Load 2 in Fig. 9 are disconnected), and the load at PCC is 540 W and 270 var. The microgrid system is originally operated in grid-connected mode with dispatched real and reactive power commands of 175 W and 75 var for each DG system (note that a PI controller is used for the reactive power control, as illustrated in Fig. 8). At $t = 1.5$ s, the microgrid is disconnected from the main grid and operates in islanding mode, and at this moment, the two DG units share the total load demand. As shown in Fig. 12(a), the real power sharing is accurate with the frequency droop method. However,

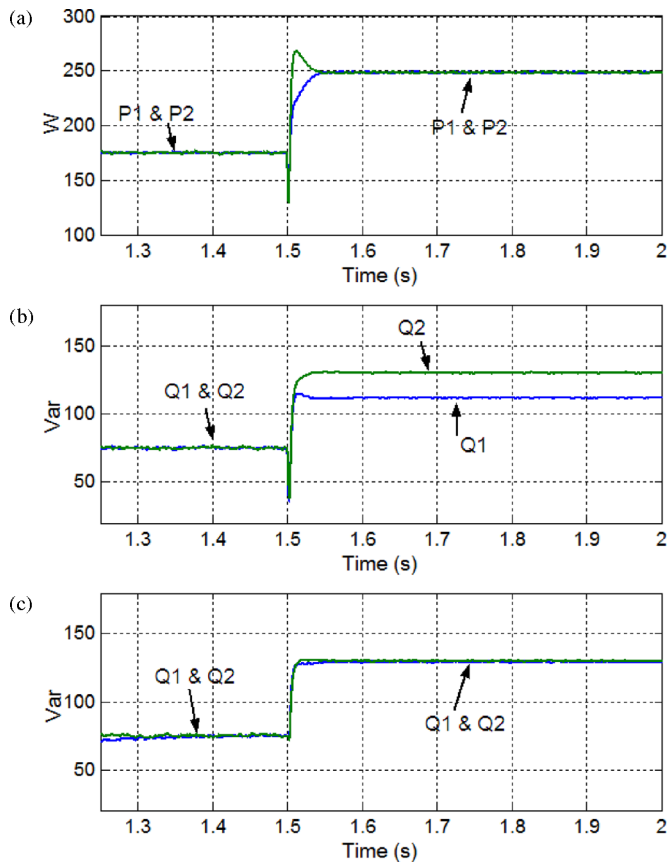

Fig. 12. Power sharing performance without DG local load. (a) Real power flows with traditional droop method. (b) Reactive power flows with traditional droop method. (c) Reactive power flows with the proposed accurate droop algorithm. (The microgrid transfers from grid-connected mode to islanding mode at $t = 1.5$ s.)

as shown in Fig. 12(b), with the traditional voltage droop control, the reactive powers produced by the two DG units are not the same due to the unequal virtual inductance implemented to the DG systems. Note that the slight real and reactive power spikes during the islanding transient associated with the traditional droop control are caused by the sudden change of voltage magnitude (see the dashed droop slopes in Fig. 7). As expected, when the proposed accurate power sharing algorithm is implemented, the reactive power control has smooth transient and accurate sharing performance, as can be seen from Fig. 12(c).

The effects of DG local loads are simulated in Fig. 13, where DG1 has a local load of 270 W and 135 var (DG2 has no local load), and the PCC load is also 270 W and 135 var. Fig. 13(a) shows the performance of reactive power sharing with the traditional droop method. It can be seen that the reactive power sharing inaccuracy becomes more severe when local load is present. Once again, with the proposed accurate sharing method, the local load effects can be accurately compensated. Note that with a 1 Ω line resistance employed in the simulation (and experiment), the real power flow has obvious effects on the local reactive power estimation accuracy. In both simulations and experiments, if the real power flow is not compensated, the estimated local reactive power offsets for the two DG units are

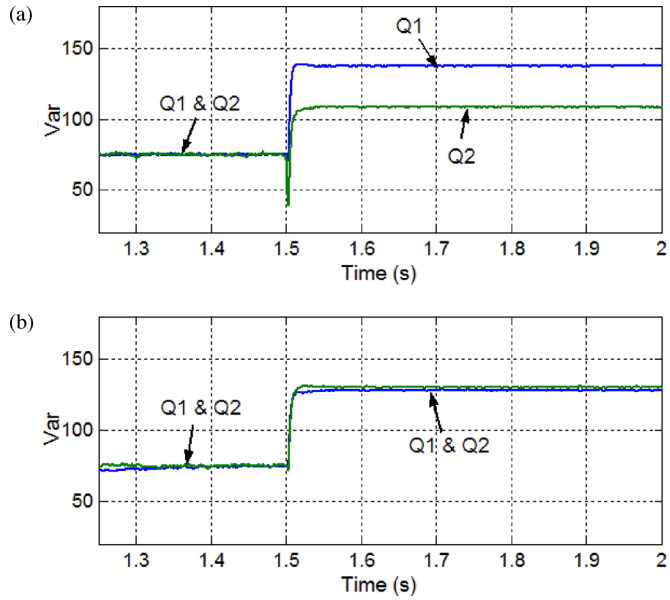

Fig. 13. Reactive power sharing with local load at DG1. (a) Traditional sharing method. (b) Proposed method. (The microgrid transfers from grid-connected mode to islanding mode at $t = 1.5$ s.)

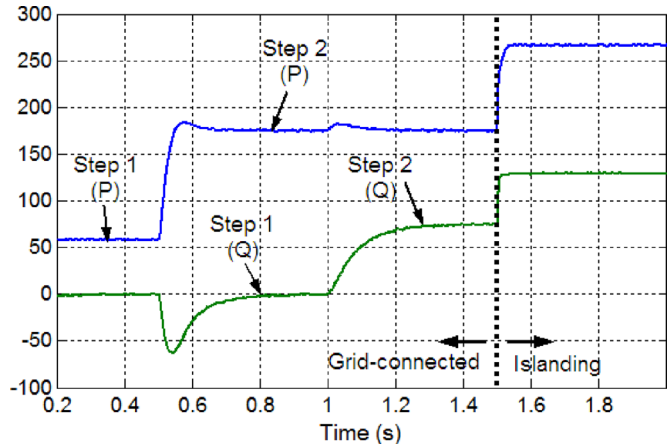

Fig. 14. Real and reactive powers during the start of DG1. (The microgrid transfers from grid-connected mode to islanding mode at $t = 1.5$ s.)

around $\{-110$ var, -205 var$\}$ without local load and $\{55$ var, -205 var$\}$ with local load at DG1. If the real power flow compensation is implemented, the estimated local reactive powers for two DG units are more accurate, which are about $\{0$ var, 0 var$\}$ without local load and $\{170$ var, 0 var$\}$ with local load at DG1.

Finally, the real and reactive power flows during the proposed start up process of DG1 in grid-connected mode are shown in Fig. 14. The two-step change of real power command (from $P^*/2$ to P^*) and two-step increase of reactive power command (from 0 to Q^*) are clearly shown. This multistep start of a DG system could accurately estimate the impedance voltage drop effects, and therefore, the accurate droop slope and the equivalent local reactive power offset.

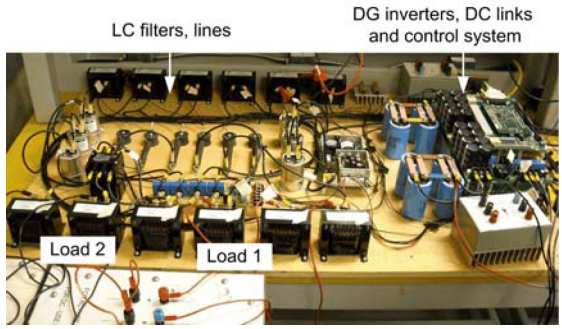

Fig. 15. Hardware microgrid system setup.

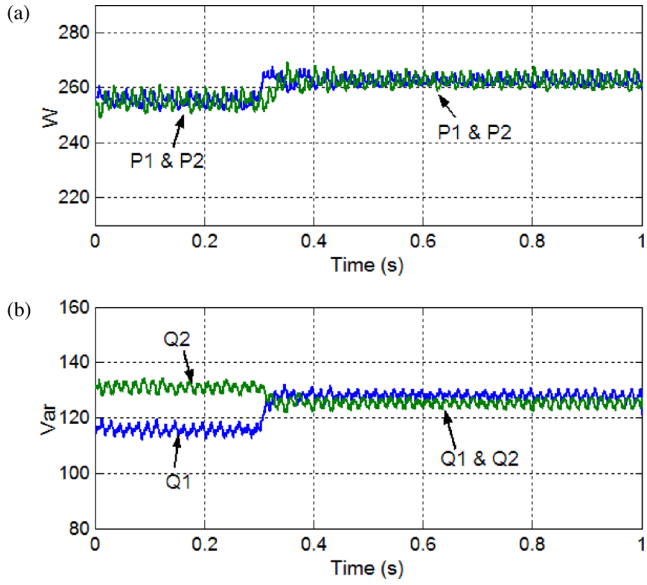

Fig. 16. Power sharing performance without DG local load. (a) Real power flows. (b) Reactive power flows. (The proposed sharing algorithm is activated at $t = 0.3$ s.)

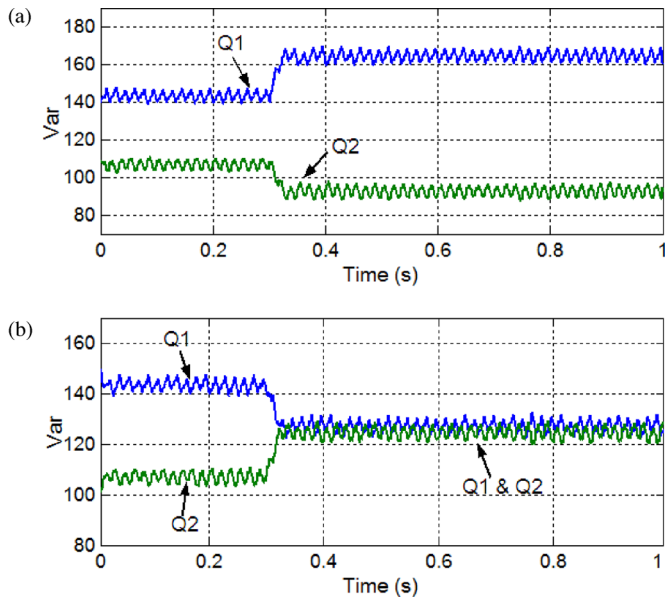

Fig. 17. Reactive power sharing with local load at DG1. (a) Without implementation of local power offset. (b) With local power compensation. (The proposed sharing algorithm with/without local power offset is activated at $t = 0.3$ s.)

TABLE II
PERFORMANCE SUMMARY OF DIFFERENT POWER CONTROL METHODS

Control methods	*Q* control algorithms *[P control are (3) and (4)]*		Performance Comparison	
	Grid-connected	Islanding	Grid-connected	Islanding
Traditional droop control method	(5) and (6)	(5) and (6)	Inaccurate Q control due to impedance voltage drops and local loads	Inaccurate Q sharing due to impedance voltage drops and local loads
Proposed power control strategy	PI (integral) control	(12), (14), (15), (19) and (20)	Accurate control of both P and Q	Accurate sharing of both P and Q

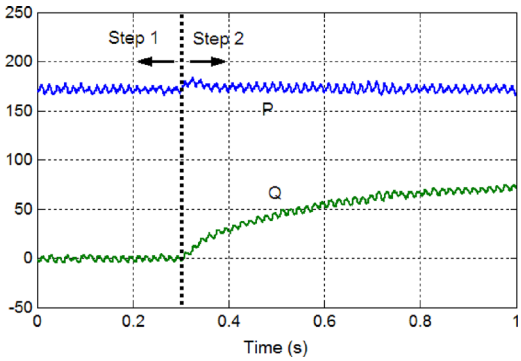

Fig. 18. Real and reactive powers during the two-step reactive power start of DG1.

IX. EXPERIMENTAL VERIFICATION

The experimental microgrid prototype with two DG units is shown in Fig. 15. The system parameters are chosen to be the same as those in simulations, and are listed in Table I. The hardware microgrid is digitally controlled by a DSP field-programmable gate array (FPGA) control system, with a TMS F2812 fixed-point DSP for implementation of the power and voltage control algorithms, and an FPGA for the space vector PWM signal generation and system protection. In the experiment, a 4.5-kVA three-phase programmable ac power supply (from California Instrument) is used to represent the stiff utility grid.

Fig. 16 shows the real and reactive power flows of the two DG systems without DG local load. The PCC load is 540 W and 270 var. The microgrid is initially operated with the traditional droop method, and it can be seen that the real power sharing is accurate but the reactive power from DG2 is higher than that from DG1 due to the unequal impedance voltage drops. At $t =$ 0.3 s, the proposed accurate power sharing algorithm is enabled and the reactive power sharing accuracy is obviously improved. It can be seen that the real powers of both DG systems are also increased slightly with the accurate sharing method. This is because the DG output voltages are properly lifted with the accurate sharing scheme (see Fig. 4 or 7).

The performance of reactive power sharing with a DG local load connected at DG1 is shown in Fig. 17. In this experiment, DG1 local load is 270 W and 135 var, and the PCC load is also 270 W and 135 var. Similarly, the microgrid is initially controlled with the traditional droop method, and DG1 shares more reactive power due to the presence of local load. In Fig. 17(a), the droop control with accurate $\Delta E/Q$ slope estimation, while without the implementation of local reactive power offset, is investigated. It can be seen that the sharing accuracy is further deteriorated if the reactive power offset is not considered. As expected, when the local load effects are properly compensated with the implementation of local reactive power offsets (170 var for DG1 and 0 for DG2), the reactive power sharing is significantly improved, as shown in Fig. 17(b).

Finally, Fig. 18 shows the two-step increase of reactive power during DG1 start in grid-connected mode, where the first step is $Q^* = 0$ and the second step is $Q^* = 75$ var (dispatched reactive power reference in grid-connected operation).

X. CONCLUSION

In this paper, a power control and sharing strategy was proposed for power-electronics-interfaced DG units in a low-voltage multibus microgrid. The proposed power control strategy contains a virtual inductor at the interfacing inverter output for real and reactive power decoupling and an accurate reactive power control and sharing algorithm with online impedance voltage drop effect estimation and local load demand effects compensation. The proposed strategy can accurately control the DG output real and reactive powers in both grid-connected mode and islanding mode without physical communications among DG units. The performance comparison between the proposed power control strategy and the traditional droop control method is summarized in Table II. Both simulation and experimental results are provided to verify the effectiveness of the proposed control strategy.

REFERENCES

[1] J. M. Carrasco, L. G. Franquelo, J. T. Bialasiewicz, E. Galvan, R. C. P. Guisado, M. A. M. Prats, J. I. Leon, and N. Moreno-Alfonso, "Power-electronic systems for the grid integration of renewable energy sources: A survey," *IEEE Trans. Power Electron.*, vol. 53, no. 4, pp. 1002–1016, Aug. 2006.

[2] R. Lasseter, "Microgrids," in *Proc. IEEE Power Eng. Soc. Winter Meet.*, 2002, pp. 305–308.

[3] M. Barnes, J. Kondoh, H. Asano, J. Oyarzabal, G. Ventakaramanan, R. Lasseter, N. Hatziargyriou, and T. Green, "Real-world microgrids—An overview," in *Proc. IEEE Int. Conf. Syst. Syst. Eng.*, Apr. 2007, pp. 1–8.

[4] Y. W. Li, D. M. Vilathgamuwa, and P. C. Loh, "Design, analysis, and real-time testing of a controller for multibus microgrid system," *IEEE Trans. Power Electron.*, vol. 19, no. 5, pp. 1195–1204, Sep. 2004.

[5] N. Pogaku, M. Prodanovic, and T. C. Green, "Modeling, analysis and testing of autonomous operation of an inverter-based microgrid," *IEEE Trans. Power Electron.*, vol. 22, no. 2, pp. 613–625, Mar. 2007.

[6] F. Katiraei and M. R. Iravani, "Power management strategies for a microgrid with multiple distributed generation units," *IEEE Trans. Power Syst.*, vol. 21, no. 4, pp. 1821–1831, Nov. 2006.

[7] F. Z. Peng, Y. W. Li, and L. M. Tolbert, "Control and protection of power electronics interfaced distributed generation systems in a customer-driven microgrid," in *Proc. IEEE Power Eng. Soc. Gen. Meet.*, 2009, pp. 1–8.
[8] M. C. Chandorkar, D. M. Divan, and R. Adapa, "Control of parallel connected inverters in standalone ac supply systems," *IEEE Trans. Ind. Appl.*, vol. 29, no. 1, pp. 136–143, Jan./Feb. 1993.
[9] E. Barklund, N. Pogaku, M. Prodanovic, C. Hernandez-Aramburo, and T. C. Green, "Energy management in autonomous microgrid using stability-constrained droop control of inverters," *IEEE Trans. Power Electron.*, vol. 23, no. 5, pp. 2346–2352, Sep. 2008.
[10] Y. A.-R. I. Mohamed and E. F. El-Saadany, "Adaptive decentralized droop controller to preserve power sharing stability of paralleled inverters in distributed generation microgrids," *IEEE Trans. Power Electron.*, vol. 23, no. 6, pp. 2806–2816, Nov. 2008.
[11] K. D. Brabandere, B. Bolsens, J. V. D. Keybus, A. Woyte, J. Driesen, and R. Belmans, "A voltage and frequency droop control method for parallel inverters," *IEEE Trans. Power Electron.*, vol. 22, no. 4, pp. 1107–1115, Jul. 2007.
[12] J. M. Guerrero, J. Matas, L. G. Vicuna, M. Castilla, and J. Miret, "Decentralized control for parallel operation of distributed generation inverters using resistive output impedance," *IEEE Trans. Ind. Electron.*, vol. 54, no. 2, pp. 994–1004, Apr. 2007.
[13] J. M. Guerrero, L. G. Vicuna, J. Matas, M. Castilla, and J. Miret, "A wireless controller to enhance dynamic performance of parallel inverters in distributed generation systems," *IEEE Trans. Power. Electron.*, vol. 19, no. 5, pp. 1205–1213, Sep. 2004.
[14] J. M. Guerrero, L. G. Vicuna, J. Matas, M. Castilla, and J. Miret, "Output impedance design of parallel-connected UPS inverters with wireless load-sharing control," *IEEE Trans. Ind. Electron.*, vol. 52, no. 4, pp. 1126–1135, Aug. 2005.
[15] A. Tuladhar, H. Jin, T. Unger, and K. Mauch, "Control of parallel inverters in distributed AC power systems with consideration of line impedance effect," *IEEE Trans. Ind. Appl.*, vol. 36, no. 1, pp. 131–138, Jan./Feb. 2000.
[16] H.-L. Jou, W.-J. Chiang, and J.-C. Wu, "A simplified control method for the grid-connected inverter with the function of islanding detection," *IEEE Trans. Power Electron.*, vol. 23, no. 6, pp. 2775–2783, Nov. 2008.
[17] Y. Li and Y. W. Li, "Decoupled power control of DG units in a power electronics interfaced low voltage microgrid," in *Proc. IEEE IPEMC*, 2009, pp. 2490–2496.
[18] M. N. Marwali, J.-W. Jung, and A. Keyhani, "Control of distributed generation systems—Part II: Load sharing control," *IEEE Trans. Power Electron.*, vol. 19, no. 6, pp. 1551–1561, Nov. 2004.
[19] M. Dai, M. N. Marwali, J.-W. Jung, and A. Keyhani, "Power flow control of a single distributed generation unit," *IEEE Trans. Power Electron.*, vol. 23, no. 1, pp. 343–352, Jan. 2008.
[20] D. N. Zmood and D. G. Holmes, "Stationary frame current regulation of PWM inverters with zero steady-state error," *IEEE Trans. Power Electron.*, vol. 18, pp. 814–822, May 2003.
[21] P. Mattavelli, "Synchronous-frame harmonic control for high-performance AC power supplies," *IEEE Trans. Ind. Appl.*, vol. 37, no. 3, pp. 864–872, May/Jun. 2001.
[22] Y. W. Li, D. M. Vilathgamuwa, and P. C. Loh, "Microgrid power quality enhancement using a three-phase four-wire grid-interfacing compensator," *IEEE Trans. Ind. Appl.*, vol. 41, no. 6, pp. 1707–1719, Nov./Dec. 2005.
[23] J. W. Kim, H. S. Choi, and B. H. Cho, "A novel droop method for converter parallel operation," *IEEE Trans. Power. Electron.*, vol. 17, no. 1, pp. 25–32, Jan. 2002.

Yun Wei Li (S'03–M'05) received the B.Sc. degree in electrical engineering from Tianjin University, Tianjin, China, in 2002, and the Ph.D. degree from Nanyang Technological University, Singapore, in 2006.

In 2005, he was a Visiting Scholar with the Institute of Energy Technology, Aalborg University, Denmark, where he worked on the medium-voltage dynamic-voltage restorer (DVR) system. From 2006 to 2007, he was a Postdoctoral Research Fellow at Ryerson University, Canada, where he was engaged in the field of the high-power converter and electric drives. In 2007, he was with Rockwell Automation Canada, where he was responsible for the development of power-factor-compensation strategies for induction motor drives. Since 2007, he has been an Assistant Professor with the Department of Electrical and Computer Engineering, University of Alberta, Edmonton, AB, Canada. His current research interests include distributed generation, microgrid, renewable energy, power quality, high-power converters, and electric motor drives.

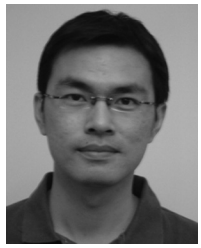

Ching-Nan Kao received the B.Sc. degree in electrical engineering from the University of Manitoba, Winnipeg, MB, Canada, in 2008. He is currently working toward the M.Eng. degree in electrical and computer engineering at the University of Alberta, Edmonton, AB, Canada.

From May to August 2008, he was an Engineering Summer Student with Westward Industries, Canada, where he was involved in hybrid vehicle design. His current research interests include power converter, hybrid vehicle, and distributed generation.